RESEARCH ARTICLE

A Hybrid Uplink Multiple Access Method Based on NOMA and SDMA

SERDAR ÖZYURT[ID]1, **ERIC PIERRE SIMON**[ID]2, **AND MURAT TORLAK**[ID]3, **(Senior Member, IEEE)**
[1]Department of Electrical and Electronics Engineering, Ankara Yıldırım Beyazıt University, 06010 Ankara, Turkey
[2]IEMN Laboratory, University of Lille, Lille, 59000 Villeneuve d'Ascq, France
[3]Department of Electrical Engineering, The University of Texas at Dallas, Richardson, TX 75080, USA

Corresponding author: Serdar Özyurt (sozyurt@ybu.edu.tr)

ABSTRACT We introduce a hybrid uplink multiple access method with a multi-antenna base station (BS) and two naive single-antenna users. Both users with no channel state information (CSI) have low computational power and simultaneously transmit their information to the receiver on the same frequency band. The CSI is assumed to be available only at the receive side. Both perfect and imperfect CSI scenarios are inspected. The decoding process at the BS relies on an adaptive combination of two eminent multiple access techniques, namely power-domain non-orthogonal multiple access and space-division multiple access. In order to reap the advantages of both approaches, the hybrid algorithm attentively switches between two multiple access methods depending on the transmit power and channels of the users. It is shown that a considerable reduction in the transmit power of the users can be attained in terms of sum rate and outage probability criteria, which are suitable performance metrics when the transmitters are not provided with any form of CSI. In addition, the investigated techniques are statistically analyzed by deriving novel and original analytical expressions for all the considered schemes.

INDEX TERMS Non-orthogonal multiple access, outage probability, space-division multiple access, sum rate, uplink.

I. INTRODUCTION

The number of devices to be connected in 5G and beyond is envisioned to soar at a skyrocketing rate with an exponentially increasing data traffic [1], [2]. Hence, it has been particularly important for the contemporary communication systems to have augmented energy and spectrum efficiency. Towards this aim, non-orthogonal multiple access (NOMA) [3] is envisaged to mature into next generation multiple access and to be an enabling technology in the upcoming communications standards [4]. Unlike the conventional orthogonal multiple access (OMA) approaches where users are assigned with orthogonal dimensions, multiple users are served within the same resource block in NOMA. To that end, the symbols of multiple users are superimposed in power-domain NOMA and successive interference cancellation (SIC) is subsequently applied at the receiver(s) to mitigate the inter-user

interference [3]. Due to its grant-free structure, NOMA also makes low transmission latency possible, which is one of the fundamental pillars in the 5G new radio (NR) air interface (around 1 ms depending on the application and deployment case). Due to its superior performance, a downlink NOMA technique (termed multiuser superposition transmission) has been inspected for the 3GPP long-term evolution (LTE) advanced (3GPP-LTE-A) networks [5]. In addition, an uplink grant-free NOMA transmission approach has been investigated for the 5G NR [6]. Although NOMA can be used for both downlink and uplink transmission cases, it is more practical and efficient to employ NOMA in uplink scenarios. This is attributed to the fact that the base station (BS) is generally armed with necessary computing power and equipment to carry out any intensive decoding process, unlike the mobile user [7]. As a potential empowering solution for 5G and beyond systems, NOMA can also be coupled with other popular enabler technologies such as beamforming, massive multiple-input multiple-output (MIMO), and

---

The associate editor coordinating the review of this manuscript and approving it for publication was Shuangqing Wei[ID].

millimeter-wave (mmWave) communications in response to ever-increasing connectivity demand. The mmWave transmission makes extremely large bandwidths with high speed data rates possible. However, these systems introduce large attenuation factors with potential blockages and high degree of directionality yielding deeply correlated channel signatures [8]. This disadvantage, on the other hand, can be exploited by NOMA in terms of easing user scheduling. By concentrating on a scenario with a single beam generated at the BS, the integration of random beamforming into a NOMA mmWave communication system is addressed in [9]. The proposed scheme is shown to significantly reduce the system overhead with important performance gains over traditional methods.

As compared to single-antenna approaches, multi-antenna methods enable substantially improved performance in terms of system capacity, communications reliability, and coverage [10]. Consequently, MIMO techniques have been utilized widely for the last two decades to mitigate the spectrum scarcity problem [11]. For instance, the currently deployed LTE-based systems allow for the employment of up to eight antennas at the BS. In addition, the use of multiple (even massive number of) antennas has been an essential element of the 5G NR from the first release [12]. Due to the fact that the standardized 5G NR systems include much shorter wavelengths, it is practically easier to install multiple antennas in these systems as compared to the previous generations. As a multiuser multi-antenna technology, space-division multiple access (SDMA), also known as multiuser MIMO, has been a major part of diverse contemporary communications standards (such as WiMAX, WiFi, LTE-A, 5G NR) under various names. In SDMA, multiple users' symbols are superimposed within the same time-frequency resource and an appropriate space-time-frequency signal processing algorithm is applied to decode the users' signals by leveraging the available spatial degrees of freedom [11].

There exist a number of studies on the combination of NOMA and SDMA approaches in the literature. It is shown that NOMA may incur a severe loss in multiplexing gain when not properly integrated into multi-antenna networks [13]. The outage performance of a downlink SDMA-NOMA single-cell cellular network is investigated in [14] under a general limited feedback framework. A dynamic user scheduling and grouping strategy is introduced where the users in distinct groups utilize different SDMA beams and those within the same group are simultaneously served by NOMA. In [15], the design of NOMA beamforming is studied in an SDMA legacy system where primary and secondary users are respectively served by SDMA and NOMA. Two beamforming strategies given by riding on existing SDMA beams and forming new beams are compared to obtain distinct trade-offs between the system performance and the complexity. As an extension of [15], a massive MIMO downlink scenario is inspected in [16] where multiple pre-arranged spatial beams are used for near-field users while NOMA is adopted to serve a certain number of additional

far-field users. A downlink mmWave communication system with a hybrid SDMA and NOMA structure is investigated in [17] and [18] by considering multiuser precoding and interference mitigation issues. In [19], a general framework based on the rate-splitting technique is introduced as a generalization of OMA, NOMA, and SDMA methods in a two-user multi-antenna broadcast channel. A similar approach is also pursued in [20] for visible light communication systems. Intelligent reflecting surface assisted downlink transmission is considered in [21] and [22] by jointly exploiting NOMA and SDMA techniques. A multi-carrier SDMA-NOMA cognitive radio system is considered in [23] to increase the number of served secondary users. In [24], the NOMA-SDMA combination is inspected to determine optimal power allocation for sum-throughput maximization in a wireless-powered communication system with sectored cells. A satellite-aerial-terrestrial network scenario is covered in [25], where multiple devices access a multi-antenna aerial platform through SDMA. In addition, the aerial platform and the earth station communicate with the satellite by means of uplink NOMA. In [26], an uplink system is inspected over an integrated satellite-aerial-terrestrial network where a high-altitude platform acting as an aerial BS with a uniform concentric ring array and multiple earth stations desire to access the satellite system relying on the NOMA assisted semi-grant-free transmission. In addition, the high-altitude platform implements SDMA to provide service to various mobile terminals. The authors of [27] investigate a combination of code-domain NOMA and SDMA approaches for low-Earth-orbit satellite Internet-of-Things systems over broadband fast fading channels. The orthogonal time frequency space waveform is utilized to accomplish connectivity with improved Doppler-robustness and decreased access latency. With the aim of achieving enhanced spectrum efficiency, an uplink mmWave massive MIMO-NOMA system is studied in [28] based on group-level SIC where SDMA is employed among users within the same group and NOMA is adopted among distinct groups.

In this work, we consider an uplink communication system with a multi-antenna BS and two single-antenna users where both users desire to simultaneously communicate with the BS on the same frequency band. It is assumed that the transmitters do not have any channel state information (CSI) and simply send their respective symbols without any power-intensive process, e.g., a wireless sensor network. In order to harvest the inherent advantages of both NOMA and SDMA methods, a hybrid approach, which adaptively switches between NOMA and SDMA decoding techniques, is adopted at the BS. According to the system parameters as the transmit power and the users' channel gains and directions, the hybrid scheme utilizes either of the two methods to decode the transmitted symbols in a reliable fashion. With respect to the BS, we cover both perfect and imperfect CSI scenarios and show that the proposed approach yields important performance gains in terms of sum rate and outage probability.
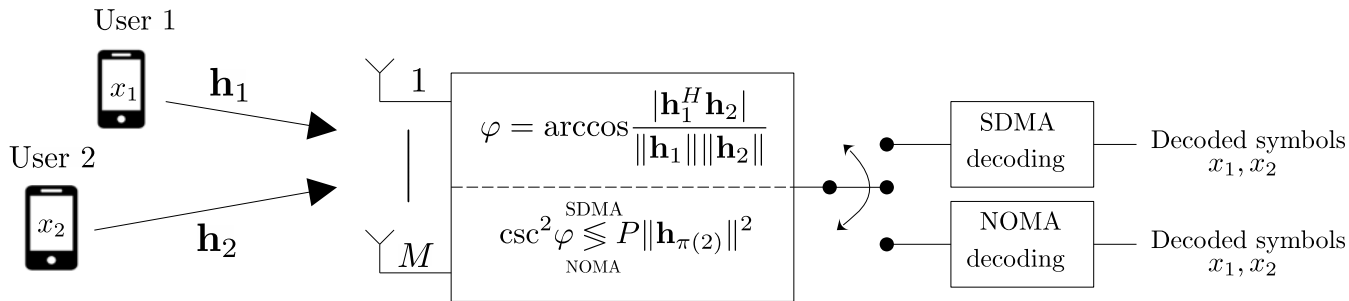
FIGURE 1. The investigated system model.

Notation: Throughout the paper, the operators $E\{.\}$, $|.|$, $(.)^H$, $\|.\|$, $\log(.)$, and $\Pr(.)$ represent the expectation, absolute value, Hermitian transpose, Euclidean norm, logarithm to base two, and probability, respectively. The matrices and column vectors are denoted by uppercase and lowercase bold letters, respectively.

The remainder of the paper is organized as follows. Section II introduces the system model and the proposed hybrid decoding algorithm. In Section III, a statistical performance analysis on all the considered schemes is carried out by deriving novel distribution expressions. The scenario with partial CSI at the receiver is investigated in Section IV and numerical results are presented in Section V. Finally, Section VI concludes the study.

II. SYSTEM MODEL

An uplink communication system with a multi-antenna BS having M ($M \geq 2$) antennas and two unsophisticated single-antenna users with low computational power is considered. Thanks to its large form-factor and computing power, equipping the BS with multiple antennas is more practical as compared to the mobile stations. Note that such a model also forms a virtual MIMO system with multiple collocated antennas at the BS and geographically dispersed single-antenna users. In order to abide by the practicality, we assume that the users do not have any kind of CSI while the BS perfectly estimates the users' channels based on the pilot signals sent from the mobile terminals.[1] A scenario with slow flat Rayleigh fading channels between the users and the BS is adopted where each user has an average power constraint of P. It is further assumed that both users are distantly separated such that their channel vectors are uncorrelated in the statistical sense. Let the channel between the kth user and the BS be represented by the $M \times 1$ vector $\mathbf{h}_k$ whose mth element stands for the fading coefficient between the kth user's antenna and the mth receive antenna at the BS. For any $k \in \{1, 2\}$, the entries of $\mathbf{h}_k$ are independent and identically distributed (IID), i.e., no antenna correlation exists. Also, each element of the vector $\mathbf{h}_k$ is a zero-mean complex Gaussian random variable with a variance of $\sigma_k^2 = d_k^{-\gamma}$ for $k \in \{1, 2\}$ where d_k and γ respectively stand for the distance from the kth user to the BS and the path loss exponent. Note that this

model is equivalent to $\mathbf{h}_k = \mathbf{u}_k d_k^{-\gamma/2}$ where the entries of $\mathbf{u}_k$ are IID zero-mean complex Gaussian random variables with unit variance [29]. For the sake of generality, the users are assumed to have distinct distances to the BS such that $d_1 < d_2$. In line with this, we label the first user as the near (cell-center) user and the second user as the far (cell-edge) user. Note that the investigated system model also represents a cellular uplink communications scenario with two clusters. The first cluster is comprised of users near the BS and the users with relatively far distances to the BS form the second cluster. By using a random scheduling policy or an OMA technique such as time-division multiple access, one user is selected from each cluster. We refer to the scheduled user(s) just as user(s) in the sequel. Within a certain frequency/time resource block, a single symbol is transmitted by each user, and the symbol sent from the kth user is denoted by x_k where $E\{|x_k|^2\} = P$. Note that such an uplink scenario where all the users transmit at the same power level is also studied in [30]. The received signal at the BS is given by

$$\mathbf{y} = \mathbf{h}_1 x_1 + \mathbf{h}_2 x_2 + \mathbf{n} \qquad (1)$$

where $\mathbf{n} \in \mathbb{C}^{M \times 1}$ denotes the additive white Gaussian noise (AWGN) at the receiver with $E\{\mathbf{n}\mathbf{n}^H\} = N_0\mathbf{I}$. Here, N_0 is the one-sided power spectral density of the AWGN at the receiver and $\mathbf{I}$ represents the identity matrix of the appropriate dimension. In addition, the entries of the vector $\mathbf{n}$ are distributed according to a zero-mean complex Gaussian distribution. In the sequel, we set $N_0 = 1$ for simplicity. A hybrid combination of SDMA and NOMA approaches is considered to carry out signal decoding process at the BS as shown in Fig. 1. For the former case, we adopt ordered zero-forcing SIC (ZF-SIC) decoding while power-domain NOMA technique is embraced in the latter scenario. Let $\{\pi(1), \pi(2)\}$ denote a permutation of $\{1, 2\}$ such that $\|\mathbf{h}_{\pi(1)}\| > \|\mathbf{h}_{\pi(2)}\|$. Under the hybrid process, the $\pi(1)$th user's symbol is first decoded and this symbol's effect is eliminated using SIC before the $\pi(2)$th user's symbol is decoded. We first explain the ordered ZF-SIC and the power-domain NOMA decoding approaches in the following.

In the first step of the ordered ZF-SIC decoding, the received signal $\mathbf{y}$ is left-multiplied by $\mathbf{h}_{\pi(1)}^H \mathbf{P}_{\mathbf{h}_{\pi(2)}}^{\perp}$ where $\mathbf{P}_{\mathbf{h}_{\pi(2)}}^{\perp}$ represents the projection matrix onto the null space of the vector $\mathbf{h}_{\pi(2)}$, i.e., $\mathbf{P}_{\mathbf{h}_{\pi(2)}}^{\perp} = \mathbf{I} - \mathbf{h}_{\pi(2)}\mathbf{h}_{\pi(2)}^H/\|\mathbf{h}_{\pi(2)}\|^2$. The

---

[1]The case where the BS only has partial CSI of the users' channels is also treated in Section IV.

$\pi(1)$th user's symbol is subsequently decoded without any intersymbol (interuser) interference. Then, the effect of this symbol is eliminated from the aggregate signal and the $\pi(2)$th user's symbol is decoded. In this case, the adopted ordering strategy is optimum in the sense that the outage probability is minimized where the outage is defined as the event that either user cannot support its target rate. It is shown in [31] that the optimum decoding order does not change the diversity order of the system and brings about 3 decibel (dB) gain in the first step receive signal-to-noise ratio (SNR) as compared to a scenario with a random decoding order. In this case, the maximum achievable average sum rate is given by

$$E\left\{C_1^{\text{SDMA}}\right\} + E\left\{C_2^{\text{SDMA}}\right\}$$

where the subscripts are used to denote the decoding order. We have

$$C_1^{\text{SDMA}} = \log\left(1 + \rho_1 P\right), \ C_2^{\text{SDMA}} = \log\left(1 + \rho_2 P\right) \quad (2)$$

with $\rho_1 = \mathbf{h}_{\pi(1)}^H \mathbf{P}_{\mathbf{h}_{\pi(2)}}^{\perp} \mathbf{h}_{\pi(1)}$ and $\rho_2 = \|\mathbf{h}_{\pi(2)}\|^2$.

Under NOMA with instantaneous ordering, the difference between the signal-to-interference-plus-noise ratios (SINRs) of the users at the BS is exploited for decoding the users' signals. To this end, the received signal vector $\mathbf{y}$ is first multiplied from left by $\mathbf{h}_{\pi(1)}^H / \|\mathbf{h}_{\pi(1)}\|$ and then $\pi(1)$th user's symbol is decoded under interference from the other user's symbol. Using SIC process, the $\pi(2)$th user's symbol is subsequently decoded in an interference-free fashion. In this case, the maximum achievable average sum rate can be written as

$$E\left\{C_1^{\text{NOMA}}\right\} + E\left\{C_2^{\text{NOMA}}\right\}$$

where

$$C_1^{\text{NOMA}} = \log\left(1 + \xi\right) \quad (3)$$

with

$$\xi = \frac{\|\mathbf{h}_{\pi(1)}\|^2 P}{\frac{|\mathbf{h}_{\pi(1)}^H \mathbf{h}_{\pi(2)}|^2}{\|\mathbf{h}_{\pi(1)}\|^2} P + 1}$$

and $C_2^{\text{NOMA}} = C_2^{\text{SDMA}}$. Consequently, the maximum achievable average sum rate of the proposed hybrid scheme is given by

$$E\left\{C_1^{\text{hybrid}}\right\} + E\left\{C_2^{\text{hybrid}}\right\}$$

where

$$C_1^{\text{hybrid}} = \max\left\{C_1^{\text{SDMA}}, C_1^{\text{NOMA}}\right\}, \ C_2^{\text{hybrid}} = C_2^{\text{SDMA}}.$$

When the channel gain disparity between the two mobile terminals is large ($\sigma_1^2 \gg \sigma_2^2$), the NOMA provides an enhanced spectral efficiency as compared to the OMA methods [3]. On the other hand, the NOMA severely suffers from an error floor when the users have similar distances to the BS. Hence, we adopt a hybrid decoding process that switches between the NOMA and the ZF-SIC techniques as outlined in Algorithm 1

Algorithm 1 Hybrid Decoding Algorithm

1: Initialization:
2: $\pi(1) = \arg\max_{k \in \{1,2\}} \|\mathbf{h}_k\|$, $\pi(2) = \arg\min_{k \in \{1,2\}} \|\mathbf{h}_k\|$,
3: $\varphi = \arccos \frac{|\mathbf{h}_1^H \mathbf{h}_2|}{\|\mathbf{h}_1\|\|\mathbf{h}_2\|}$
4: **if** $\csc^2 \varphi \le P \|\mathbf{h}_{\pi(2)}\|^2$ **then**
5:      Perform SDMA decoding:
6:      Apply $\mathbf{h}_{\pi(1)}^H \mathbf{P}_{\mathbf{h}_{\pi(2)}}^{\perp} \mathbf{y}$ and decode the $\pi(1)$th user's symbol.
7: **else**
8:      Perform NOMA decoding:
9:      Apply $\mathbf{h}_{\pi(1)}^H \mathbf{y} / \|\mathbf{h}_{\pi(1)}\|$ and decode the $\pi(1)$th user's symbol.
10: **end if**
11: Apply SIC and decode the $\pi(2)$th user's symbol.
12: **return** Decoded symbols

---

in response to the changes in the users' channel parameters. To this end, we utilize the following theorem.

Theorem 1: Let φ be the Hermitian angle between the users' channel vectors $\mathbf{h}_1$ and $\mathbf{h}_2$ such that $0 \le \varphi \le \frac{\pi}{2}$ [32]. We have

$$\varphi = \arccos \frac{|\mathbf{h}_1^H \mathbf{h}_2|}{\|\mathbf{h}_1\| \|\mathbf{h}_2\|}. \quad (4)$$

The instantaneous sum rate that can be supported under SDMA (ZF-SIC) decoding is no less than that of under NOMA decoding if and only if

$$\csc^2 \varphi \le P \min\left\{\|\mathbf{h}_1\|^2, \|\mathbf{h}_2\|^2\right\} \quad (5)$$

where csc(.) denotes the cosecant function.

Proof: Using the rate expressions in (2) and (3), we can conclude that the instantaneous sum rate under SDMA (ZF-SIC) decoding is no less than that of under NOMA decoding only if

$$\mathbf{h}_{\pi(1)}^H \mathbf{P}_{\mathbf{h}_{\pi(2)}}^{\perp} \mathbf{h}_{\pi(1)} P \ge \frac{\|\mathbf{h}_{\pi(1)}\|^2 P}{\frac{|\mathbf{h}_{\pi(1)}^H \mathbf{h}_{\pi(2)}|^2}{\|\mathbf{h}_{\pi(1)}\|^2} P + 1}. \quad (6)$$

We have

$$\mathbf{h}_{\pi(1)}^H \mathbf{P}_{\mathbf{h}_{\pi(2)}}^{\perp} \mathbf{h}_{\pi(1)} = \|\mathbf{h}_{\pi(1)}\|^2 - \frac{|\mathbf{h}_{\pi(1)}^H \mathbf{h}_{\pi(2)}|^2}{\|\mathbf{h}_{\pi(2)}\|^2}. \quad (7)$$

Substituting (7) into (6) and then using (4), we can write

$$1 - \cos^2 \varphi \ge \frac{1}{P \|\mathbf{h}_{\pi(2)}\|^2 \cos^2 \varphi + 1} \quad (8)$$

where $\cos^2 \varphi$ gives a measure on the orthogonality between $\mathbf{h}_1$ and $\mathbf{h}_2$. Inverting both sides, (8) can also be expressed as follows

$$\sin^{-2} \varphi \le P \|\mathbf{h}_{\pi(2)}\|^2 \cos^2 \varphi + 1. \quad (9)$$

Using the trigonometric identities together with the fact that $\|\mathbf{h}_{\pi(2)}\|^2 = \min\{\|\mathbf{h}_1\|^2, \|\mathbf{h}_2\|^2\}$, the preceding inequality can easily be simplified into the desired expression. ∎

The probability density function (PDF) of φ is given by

$$f_\varphi(\varphi) = 2(M-1)\cos\varphi\,(\sin\varphi)^{2M-3} \tag{10}$$

for $0 \leq \varphi \leq \pi/2$ [31]. It is worth to inspecting two extreme scenarios. When the channel directions are close to being orthogonal, then both $\|\mathbf{h}_1\|^2$ and $\|\mathbf{h}_2\|^2$ are required to be sufficiently larger than $1/P$ for the SDMA decoding to yield a superior sum rate. On the other hand, if the channel directions are nearly parallel such that $\cos^2\varphi = (1-\epsilon)$ with ϵ representing an accordingly small positive quantity, then the SDMA decoding attains a larger sum rate only when $\min\{\|\mathbf{h}_1\|^2, \|\mathbf{h}_2\|^2\} \geq 1/(\epsilon P)$. The inner product between two normalized complex vectors representing channel directions is also used in [33] and [34] as a decision metric to carry out a semi-orthogonal user selection process. It is also utilized to model the channel quantization error with limited feedback and user scheduling in [35], where the square of the sine of the Hermitian angle between the actual and quantized channel directions equals the quantization error.

III. PERFORMANCE ANALYSIS

In this section, we present a statistical analysis on the maximum achievable average sum rate and the outage probability of the proposed hybrid scheme where the outage is defined as the event either of the users' target rates cannot be supported. To this end, we determine the corresponding cumulative distribution function (CDF) expressions of the received SNR (and SINR) values for the hybrid scheme as well as for the original SDMA and NOMA techniques. The derived analytical results on the SDMA and NOMA approaches are also novel and provide original contribution to the literature. We approximate the average sum rate and the outage probability by interchanging the order of maximization and the expectation and by utilizing the Boole's inequality (also known as the union bound) in the former and latter cases, respectively. As shown in Section V, both approximations turn out to be quite tight. Let $R_k^{\text{SDMA}}, R_k^{\text{NOMA}}$, and R_k^{hybrid} stand for the target rates corresponding to the kth decoded user under SDMA, NOMA, and the proposed hybrid approaches, respectively. The outage probability is given by

$$P_{\text{out}}^{\text{SDMA}} = \Pr\left(C_1^{\text{SDMA}} < R_1^{\text{SDMA}} \text{ or } C_2^{\text{SDMA}} < R_2^{\text{SDMA}}\right)$$

and

$$P_{\text{out}}^{\text{NOMA}} = \Pr\left(C_1^{\text{NOMA}} < R_1^{\text{NOMA}} \text{ or } C_2^{\text{NOMA}} < R_2^{\text{NOMA}}\right)$$

for SDMA and NOMA, respectively. We can approximately write

$$P_{\text{out}}^{\text{SDMA}} = \Pr\left(C_1^{\text{SDMA}} < R_1^{\text{SDMA}}\right) + \Pr\left(C_2^{\text{SDMA}} < R_2^{\text{SDMA}}\right)$$

and

$$P_{\text{out}}^{\text{NOMA}} = \Pr\left(C_1^{\text{NOMA}} < R_1^{\text{NOMA}}\right) + \Pr\left(C_2^{\text{NOMA}} < R_2^{\text{NOMA}}\right).$$

Using (2) and (3), we can write

$$\Pr\left(C_1^{\text{SDMA}} < R_1^{\text{SDMA}}\right) = F_{\rho_1}\left(\frac{2^{R_1^{\text{SDMA}}}-1}{P}\right),$$

$$\Pr\left(C_2^{\text{SDMA}} < R_2^{\text{SDMA}}\right) = F_{\rho_2}\left(\frac{2^{R_2^{\text{SDMA}}}-1}{P}\right),$$

$$\Pr\left(C_1^{\text{NOMA}} < R_1^{\text{NOMA}}\right) = F_\xi\left(2^{R_1^{\text{NOMA}}}-1\right),$$

$$\Pr\left(C_2^{\text{NOMA}} < R_2^{\text{NOMA}}\right) = F_{\rho_2}\left(\frac{2^{R_2^{\text{NOMA}}}-1}{P}\right).$$

Here, $F_{\rho_1}(.)$, $F_{\rho_2}(.)$, and $F_\xi(.)$ represent the CDFs of ρ_1, ρ_2, and ξ, respectively. The variables $\|\mathbf{h}_1\|^2$ and $\|\mathbf{h}_2\|^2$ are independent (but non-identically distributed) weighted chi-squared random variables each with $2M$ degrees of freedom such that

$$F_{\|\mathbf{h}_1\|^2}(\eta_1) = 1 - \frac{\Gamma\left(M, \eta_1/\sigma_1^2\right)}{\Gamma(M)} \tag{11}$$

for $\eta_1 \geq 0$ and

$$F_{\|\mathbf{h}_2\|^2}(\eta_2) = 1 - \frac{\Gamma\left(M, \eta_2/\sigma_2^2\right)}{\Gamma(M)} \tag{12}$$

for $\eta_2 \geq 0$ [33]. In (11) and (12), $\Gamma(.)$ and $\Gamma(.,.)$ respectively represent the gamma function and the incomplete gamma function [36].

Exploiting the properties of the null projection, it can be shown that $\rho_1 = \max\{\|\mathbf{h}_1\|^2, \|\mathbf{h}_2\|^2\}\sin^2\varphi$. Using this fact together with (11) and (12), we can write

$$F_{\rho_1}(\rho_1) = \int_0^{\pi/2} F_{\|\mathbf{h}_1\|^2}\left(\frac{\rho_1}{\sin^2\varphi}\right) F_{\|\mathbf{h}_2\|^2}\left(\frac{\rho_1}{\sin^2\varphi}\right) f_\varphi(\varphi)\,d\varphi \tag{13}$$

for $\rho_1 \geq 0$. Also, utilizing $\rho_2 = \min\{\|\mathbf{h}_1\|^2, \|\mathbf{h}_2\|^2\}$, it follows that

$$F_{\rho_2}(\rho_2) = 1 - \left(1 - F_{\|\mathbf{h}_1\|^2}(\rho_2)\right)\left(1 - F_{\|\mathbf{h}_2\|^2}(\rho_2)\right) \tag{14}$$

for $\rho_2 \geq 0$. Using (10), (11), and (12) in (13) and (14), we can write

$$F_{\rho_1}(\rho_1)$$
$$= 1 - (M-1)\left[\sum_{k=0}^{M-1}\left(\frac{E_{M-k}\left(\frac{\rho_1}{\sigma_1^2}\right)}{\rho_1^{-k}\,k!\,\sigma_1^{2k}} + \frac{E_{M-k}\left(\frac{\rho_1}{\sigma_2^2}\right)}{\rho_1^{-k}\,k!\,\sigma_2^{2k}}\right)\right]$$
$$+ (M-1)\left[\sum_{k_1=0}^{M-1}\sum_{k_2=0}^{M-1}\frac{E_{M-k_1-k_2}\left(\frac{\rho_1}{\sigma_1^2}+\frac{\rho_1}{\sigma_2^2}\right)}{\rho_1^{-k_1-k_2}\,k_1!\,k_2!\,\sigma_1^{2k_1}\,\sigma_2^{2k_2}}\right] \tag{15}$$

and

$$F_{\rho_2}(\rho_2) = 1 - \frac{\Gamma\left(M, \rho_2/\sigma_1^2\right)\Gamma\left(M, \rho_2/\sigma_2^2\right)}{(\Gamma(M))^2} \quad (16)$$

for $\rho_1 \geq 0$ and $\rho_2 \geq 0$.

In (15),

$$E_n(z) = \int_1^\infty \frac{e^{-zt}}{t^n}\, dt = z^{n-1}\,\Gamma(1-n, z)$$

denotes the exponential integral function [36]. The CDF $F_\xi(\xi)$ can be expressed as follows

$$F_\xi(\xi) = \Pr\left(\|\mathbf{h}_{\pi(1)}\|^2 \leq \xi\left(\frac{|\mathbf{h}_{\pi(1)}^H \mathbf{h}_{\pi(2)}|^2}{\|\mathbf{h}_{\pi(1)}\|^2} + \frac{1}{P}\right)\right)$$
$$= \Pr\left(\|\mathbf{h}_{\pi(1)}\|^2 \leq \|\mathbf{h}_{\pi(2)}\|^2 \xi \cos^2\varphi + \xi/P\right) \quad (17)$$

for $\xi \geq 0$. The evaluation of the preceding probability entails the joint PDF of $\|\mathbf{h}_{\pi(1)}\|^2$, $\|\mathbf{h}_{\pi(2)}\|^2$, and $\cos^2\varphi$. Using the tools from order statistics [37], we can conclude that

$$f_{\|\mathbf{h}_{\pi(1)}\|^2,\,\|\mathbf{h}_{\pi(2)}\|^2}(\alpha_1, \alpha_2) = \frac{e^{-\frac{\alpha_1\sigma_1^2 + \alpha_2\sigma_2^2}{\sigma_1^2\sigma_2^2}} + e^{-\frac{\alpha_1\sigma_2^2 + \alpha_2\sigma_1^2}{\sigma_1^2\sigma_2^2}}}{(\alpha_1\alpha_2)^{1-M}\left(\sigma_1^2\sigma_2^2\right)^M (\Gamma(M))^2} \quad (18)$$

for $\alpha_1 \geq \alpha_2 \geq 0$. In addition, the random variable $\cos^2\varphi$ is independent from $\|\mathbf{h}_{\pi(1)}\|^2$ and $\|\mathbf{h}_{\pi(2)}\|^2$. Its PDF can be derived from (10) as follows

$$f_{\cos^2\varphi}(\beta) = (M-1)(1-\beta)^{M-2} \quad (19)$$

for $0 \leq \beta \leq 1$.

Let $\Xi(\alpha_1, \alpha_2, \beta) = f_{\|\mathbf{h}_{\pi(1)}\|^2,\,\|\mathbf{h}_{\pi(2)}\|^2}(\alpha_1, \alpha_2)\, f_{\cos^2\varphi}(\beta)$. Using (17), we can write

$$F_\xi(\xi) = \begin{cases} I_1 & \text{for } 0 \leq \xi < 1, \\ I_2 + I_3 & \text{for } \xi \geq 1, \end{cases} \quad (20)$$

where

$$I_1 = \int_0^1 \int_0^{\frac{\xi/P}{1-\xi\beta}} \int_{\alpha_2}^{\left(\alpha_2\xi\beta + \frac{\xi}{P}\right)} \Xi(\alpha_1, \alpha_2, \beta)\, d\alpha_1\, d\alpha_2\, d\beta,$$

$$I_2 = \int_0^{1/\xi} \int_0^{\frac{\xi/P}{1-\xi\beta}} \int_{\alpha_2}^{\left(\alpha_2\xi\beta + \frac{\xi}{P}\right)} \Xi(\alpha_1, \alpha_2, \beta)\, d\alpha_1\, d\alpha_2\, d\beta,$$

$$I_3 = \int_{1/\xi}^1 \int_0^\infty \int_{\alpha_2}^{\left(\alpha_2\xi\beta + \frac{\xi}{P}\right)} \Xi(\alpha_1, \alpha_2, \beta)\, d\alpha_1\, d\alpha_2\, d\beta.$$

Utilizing (18) and (19), exact closed-forms results can be obtained on I_1, I_2, and I_3 for a set of $\{M, P, \sigma_1^2, \sigma_2^2\}$ values. These expressions are omitted here for the sake of fluency. The maximum achievable average sum rate of the hybrid scheme can be written approximately as follows

$$\max\{\mathrm{E}\{\log(1+\rho_1 P)\}, \mathrm{E}\{\log(1+\xi)\}\} + \mathrm{E}\{\log(1+\rho_2 P)\}, \quad (21)$$

which can be evaluated by using the acquired CDF expressions in (15), (16), and (20).

Let $P_{\text{out}}^{\text{hybrid}}$ denote the outage probability of the proposed hybrid scheme. We have

$$P_{\text{out}}^{\text{hybrid}} = \Pr\left(C_1^{\text{hybrid}} < R_1^{\text{hybrid}} \text{ or } C_2^{\text{hybrid}} < R_2^{\text{hybrid}}\right)$$
$$= \Pr\left(C_1^{\text{hybrid}} < R_1^{\text{hybrid}}\right) + \Pr\left(C_2^{\text{hybrid}} < R_2^{\text{hybrid}}\right)$$
$$= \Pr\left(\max\left\{C_1^{\text{SDMA}},\, C_1^{\text{NOMA}}\right\} < R_1^{\text{hybrid}}\right)$$
$$+ F_{\rho_2}\left(\frac{2^{R_2^{\text{hybrid}}} - 1}{P}\right). \quad (22)$$

Define

$$\Psi(\mu_1, \mu_2, \mu_3, \mu_4)$$
$$= \int_{\mu_1}^{\mu_2} \int_{\mu_3}^{\mu_4} \int_{\frac{P\alpha_1-\lambda}{P\lambda\alpha_2}}^1 \Xi(\alpha_1, \alpha_2, \beta)\, d\beta\, d\alpha_1\, d\alpha_2,$$

$$\Phi(\mu_1, \mu_2, \mu_3, \mu_4)$$
$$= \int_{\mu_1}^{\mu_2} \int_{\mu_3}^{\mu_4} \int_{1-\frac{\lambda}{P\alpha_1}}^1 \Xi(\alpha_1, \alpha_2, \beta)\, d\beta\, d\alpha_1\, d\alpha_2,$$

with $\lambda = (2^{R_1^{\text{hybrid}}} - 1)$. Then, using (2) and (3), the probability $\Pr\left(\max\left\{C_1^{\text{SDMA}}, C_1^{\text{NOMA}}\right\} < R_1^{\text{hybrid}}\right)$ can be written as

$$\Pr\left(\cos^2\varphi > \frac{P\|\mathbf{h}_{\pi(1)}\|^2 - \lambda}{P\|\mathbf{h}_{\pi(2)}\|^2\lambda},\ \cos^2\varphi > 1 - \frac{\lambda}{P\|\mathbf{h}_{\pi(1)}\|^2}\right)$$
$$= \begin{cases} \Upsilon_1 - \Upsilon_2 + F_{\|\mathbf{h}_{\pi(1)}\|^2,\,\|\mathbf{h}_{\pi(2)}\|^2}(\frac{\lambda}{P}, \frac{\lambda}{P}) & \text{for } 0 \leq \lambda < 1, \\ \Upsilon_3 + \Upsilon_4 - \Upsilon_5 - \Upsilon_6 + F_{\|\mathbf{h}_{\pi(1)}\|^2,\,\|\mathbf{h}_{\pi(2)}\|^2}(\frac{\lambda}{P}, \frac{\lambda}{P}) & \text{for } \lambda \geq 1. \end{cases}$$
$$(23)$$

In (23), we have

$$\Upsilon_1 = \Psi\left(0, \frac{\lambda}{P(1-\lambda)}, \alpha_2, \lambda\alpha_2 + \frac{\lambda}{P}\right),\ \Upsilon_2 = \Psi\left(0, \frac{\lambda}{P}, \alpha_2, \frac{\lambda}{P}\right),$$
$$\Upsilon_3 = \Psi\left(0, \infty, \lambda\alpha_2, \lambda\alpha_2 + \frac{\lambda}{P}\right),\ \Upsilon_4 = \Phi\left(\frac{1}{P}, \infty, \alpha_2, \lambda\alpha_2\right),$$
$$\Upsilon_5 = \Psi\left(0, \frac{1}{P}, \lambda\alpha_2, \frac{\lambda}{P}\right),\ \text{and}\ \Upsilon_6 = \Phi\left(\frac{1}{P}, \frac{\lambda}{P}, \alpha_2, \frac{\lambda}{P}\right).$$

In addition, $F_{\|\mathbf{h}_{\pi(1)}\|^2,\,\|\mathbf{h}_{\pi(2)}\|^2}(\lambda/P, \lambda/P)$ equals the joint CDF of $\|\mathbf{h}_{\pi(1)}\|^2$ and $\|\mathbf{h}_{\pi(2)}\|^2$ evaluated at the point $\{\lambda/P, \lambda/P\}$, i.e.,

$$\int_0^{\frac{\lambda}{P}} \int_{\alpha_2}^{\frac{\lambda}{P}} f_{\|\mathbf{h}_{\pi(1)}\|^2,\,\|\mathbf{h}_{\pi(2)}\|^2}(\alpha_1, \alpha_2)\, d\alpha_1\, d\alpha_2.$$

The analytical solutions to the preceding integrals can be obtained by substituting the corresponding $\{\lambda, M, P, \sigma_1^2, \sigma_2^2\}$ values.

It is instructive to investigate how frequently the hybrid scheme switches between two decoding approaches. To this end, we examine the probability that the instantaneous sum rate with SDMA decoding is greater than or equal to that of under NOMA decoding. Elaborating on (5) by using the properties of the null projection, this probability can be shown to be equivalent to the CDF of $\Omega = 1/\left(\min\left\{\|\mathbf{h}_1\|^2, \|\mathbf{h}_2\|^2\right\} \sin^2 \varphi\right)$ evaluated at P, i.e., $F_\Omega(P)$. We can write

$$F_\Omega(\omega) = \int_0^{\pi/2} \left(1 - F_{\|\mathbf{h}_1\|^2}\left(\frac{1}{\omega \sin^2 \varphi}\right)\right)$$
$$\left(1 - F_{\|\mathbf{h}_2\|^2}\left(\frac{1}{\omega \sin^2 \varphi}\right)\right) f_\varphi(\varphi)\, d\varphi \quad (24)$$

for $\omega \geq 0$. Substituting (10), (11), and (12) into (24) and evaluating the resulting integral, it can be shown that

$$F_\Omega(\omega) = (M - 1) \sum_{k_1=0}^{M-1} \sum_{k_2=0}^{M-1} \frac{E_{M-k_1-k_2}\left(\frac{\sigma_1^2 + \sigma_2^2}{\omega\, \sigma_1^2\, \sigma_2^2}\right)}{\omega^{k_1+k_2}\, k_1!\, k_2!\, \sigma_1^{2k_1}\, \sigma_2^{2k_2}}$$
$$(25)$$

for $\omega \geq 0$.

IV. PARTIAL CSI AT THE BS

In this section, we cover the scenario where the users do not have any kind of CSI while the BS has partial (imperfect) CSI of the users' channels. To that end, the BS's estimate for the kth user's channel (denoted by $\widetilde{\mathbf{h}}_k$) is modeled in a widely adopted practical fashion as follows

$$\widetilde{\mathbf{h}}_k = \vartheta\, \mathbf{h}_k + \sqrt{1 - \vartheta^2}\, \mathbf{z}_k. \quad (26)$$

Here, $\mathbf{h}_k$ stands for the kth user's actual channel (as defined in Section II) and the estimation error vector $\mathbf{z}_k$ has the same distribution as $\mathbf{h}_k$ but uncorrelated with it. In addition, ϑ is the correlation coefficient between the true and estimated channel vectors for the kth user. It is given by

$$\vartheta = \frac{\left|\mathrm{E}\left\{\widetilde{\mathbf{h}}_k^H \mathbf{h}_k\right\}\right|}{\sqrt{\mathrm{E}\left\{\|\mathbf{h}_k\|^2\right\} \mathrm{E}\left\{\|\widetilde{\mathbf{h}}_k\|^2\right\}}} \quad (27)$$

for $0 \leq \vartheta \leq 1$. The decoding process at the BS is carried out in an analogous manner as in Section II based on the estimated channel vectors. The actual channels of the users are accordingly replaced with the estimated ones in Algorithm 1. In addition, the hybrid algorithm switches to SDMA if $\csc^2 \varphi \leq \vartheta^2 P \|\widetilde{\mathbf{h}}_{\pi(2)}\|^2$, and vice versa. In order to justify this switching condition and to express the resulting SINR and SNR values in terms of the estimated channel vectors, we tweak the model in (26) as $\mathbf{h}_k = \vartheta\, \widetilde{\mathbf{h}}_k + \sqrt{1 - \vartheta^2}\, \mathbf{e}_k$ for $k \in \{1, 2\}$ without altering the statistics of $\mathbf{h}_k$ and $\widetilde{\mathbf{h}}_k$. Here, $\mathbf{e}_k$ is identically distributed with $\widetilde{\mathbf{h}}_k$ and uncorrelated with it. Hence, the correlation coefficient between the true and estimated channel vectors is also equal to ϑ in this

case. The $\pi(1)$th user's symbol is initially decoded and this symbol's effect is removed by using SIC before the $\pi(2)$th user's symbol is decoded where $\|\widetilde{\mathbf{h}}_{\pi(1)}\| > \|\widetilde{\mathbf{h}}_{\pi(2)}\|$. With the ordered ZF-SIC decoding, the received signal $\mathbf{y}$ is first left-multiplied by $\widetilde{\mathbf{h}}_{\pi(1)}^H \mathbf{P}_{\widetilde{\mathbf{h}}_{\pi(2)}}^\perp$ to decode the $\pi(1)$th user's symbol. Here, $\mathbf{P}_{\widetilde{\mathbf{h}}_{\pi(2)}}^\perp$ denotes the projection matrix onto the null space of the vector $\widetilde{\mathbf{h}}_{\pi(2)}$. On the other hand, $\mathbf{y}$ is initially multiplied from left by $\widetilde{\mathbf{h}}_{\pi(1)}^H / \|\widetilde{\mathbf{h}}_{\pi(1)}\|$ to decode the $\pi(1)$th user's symbol under NOMA with instantaneous ordering. The maximum achievable average sum rates are correspondingly given by

$$\mathrm{E}\left\{\widetilde{C}_1^{\mathrm{SDMA}}\right\} + \mathrm{E}\left\{\widetilde{C}_2^{\mathrm{SDMA}}\right\}$$

and

$$\mathrm{E}\left\{\widetilde{C}_1^{\mathrm{NOMA}}\right\} + \mathrm{E}\left\{\widetilde{C}_2^{\mathrm{NOMA}}\right\}$$

for SDMA and NOMA decoding processes, respectively. Here, we have

$$\widetilde{C}_1^{\mathrm{SDMA}} = \log\left(1 + \Delta_1\right), \quad \widetilde{C}_1^{\mathrm{NOMA}} = \log\left(1 + \Delta_2\right),$$

and

$$\widetilde{C}_2^{\mathrm{SDMA}} = \widetilde{C}_2^{\mathrm{NOMA}} = \log\left(1 + \Delta_3\right)$$

where

$$\Delta_1 = \frac{\left|\widetilde{\mathbf{h}}_{\pi(1)}^H \mathbf{P}_{\widetilde{\mathbf{h}}_{\pi(2)}}^\perp \mathbf{h}_{\pi(1)}\right|^2 P}{\left|\widetilde{\mathbf{h}}_{\pi(1)}^H \mathbf{P}_{\widetilde{\mathbf{h}}_{\pi(2)}}^\perp \mathbf{h}_{\pi(2)}\right|^2 P + \widetilde{\mathbf{h}}_{\pi(1)}^H \mathbf{P}_{\widetilde{\mathbf{h}}_{\pi(2)}}^\perp \widetilde{\mathbf{h}}_{\pi(1)}}, \quad (28)$$

$$\Delta_2 = \frac{\left|\widetilde{\mathbf{h}}_{\pi(1)}^H \mathbf{h}_{\pi(1)}\right|^2 P}{\left|\widetilde{\mathbf{h}}_{\pi(1)}^H \mathbf{h}_{\pi(2)}\right|^2 P + \|\widetilde{\mathbf{h}}_{\pi(1)}\|^2}, \quad (29)$$

and

$$\Delta_3 = \frac{\left|\widetilde{\mathbf{h}}_{\pi(2)}^H \mathbf{h}_{\pi(2)}\right|^2 P}{\|\widetilde{\mathbf{h}}_{\pi(2)}\|^2}. \quad (30)$$

We can write

$$\Delta_1 = \frac{\left|\vartheta\, \widetilde{\mathbf{h}}_{\pi(1)}^H \mathbf{P}_{\widetilde{\mathbf{h}}_{\pi(2)}}^\perp \widetilde{\mathbf{h}}_{\pi(1)} + \sqrt{1 - \vartheta^2}\, \widetilde{\mathbf{h}}_{\pi(1)}^H \mathbf{P}_{\widetilde{\mathbf{h}}_{\pi(2)}}^\perp \mathbf{e}_{\pi(1)}\right|^2}{(1 - \vartheta^2)\left|\widetilde{\mathbf{h}}_{\pi(1)}^H \mathbf{P}_{\widetilde{\mathbf{h}}_{\pi(2)}}^\perp \mathbf{e}_{\pi(2)}\right|^2 + \frac{\widetilde{\mathbf{h}}_{\pi(1)}^H \mathbf{P}_{\widetilde{\mathbf{h}}_{\pi(2)}}^\perp \widetilde{\mathbf{h}}_{\pi(1)}}{P}},$$

$$\Delta_2 = \frac{\left|\vartheta\, \|\widetilde{\mathbf{h}}_{\pi(1)}\|^2 + \sqrt{1 - \vartheta^2}\, \widetilde{\mathbf{h}}_{\pi(1)}^H \mathbf{e}_{\pi(1)}\right|^2}{\left|\vartheta\, \widetilde{\mathbf{h}}_{\pi(1)}^H \widetilde{\mathbf{h}}_{\pi(2)} + \sqrt{1 - \vartheta^2}\, \widetilde{\mathbf{h}}_{\pi(1)}^H \mathbf{e}_{\pi(2)}\right|^2 + \frac{\|\widetilde{\mathbf{h}}_{\pi(1)}\|^2}{P}},$$

$$\Delta_3 = \frac{\left|\vartheta\, \|\widetilde{\mathbf{h}}_{\pi(2)}\|^2 + \sqrt{1 - \vartheta^2}\, \widetilde{\mathbf{h}}_{\pi(2)}^H \mathbf{e}_{\pi(2)}\right|^2 P}{\|\widetilde{\mathbf{h}}_{\pi(2)}\|^2}.$$

In practice, ϑ equals a real number that is usually near to the unity depending on the estimation precision. Therefore, we accordingly approximate Δ_1, Δ_2, and Δ_3 by neglecting

TABLE 1. Simulation parameters.

	Number of BS antennas	σ_1^2	σ_2^2	R_{1t}	R_{2t}	CSI at BS
Fig. 2	$2 \leq M \leq 10$	0 dB	-35 dB	N/A	N/A	Perfect ($\vartheta = 1$)
Fig. 3	$M \in \{2, 6\}$	0 dB	$\in \{-30, -40\}$ dB	N/A	N/A	Perfect ($\vartheta = 1$)
Fig. 4	$M = 2$	0 dB	$\in \{-30, -40\}$ dB	8 bits/s/Hz	$\in \{1, 0.5\}$ bits/s/Hz	Perfect ($\vartheta = 1$)
Fig. 5	$M \in \{2, 6\}$	0 dB	$\in \{-20, -30, -40\}$ dB	N/A	N/A	Perfect ($\vartheta = 1$)
Fig. 6	$M = 2$	0 dB	-30 dB	4 bits/s/Hz	0.5 bits/s/Hz	Possibly imperfect ($\vartheta \in \{0.95, 0.99, 1\}$)

the terms that contain $(1 - \vartheta^2)$ (or $\sqrt{1 - \vartheta^2}$) as follows

$$\Delta_1 = \frac{\vartheta^2 \left(\widetilde{\mathbf{h}}_{\pi(1)}^H \mathbf{P}_{\widetilde{\mathbf{h}}_{\pi(2)}}^{\perp} \widetilde{\mathbf{h}}_{\pi(1)} \right)^2}{\dfrac{\widetilde{\mathbf{h}}_{\pi(1)}^H \mathbf{P}_{\widetilde{\mathbf{h}}_{\pi(2)}}^{\perp} \widetilde{\mathbf{h}}_{\pi(1)}}{P}} = \vartheta^2 P \, \widetilde{\mathbf{h}}_{\pi(1)}^H \mathbf{P}_{\widetilde{\mathbf{h}}_{\pi(2)}}^{\perp} \widetilde{\mathbf{h}}_{\pi(1)},$$

$$\Delta_2 = \frac{\vartheta^2 \|\widetilde{\mathbf{h}}_{\pi(1)}\|^4}{\vartheta^2 |\widetilde{\mathbf{h}}_{\pi(1)}^H \widetilde{\mathbf{h}}_{\pi(2)}|^2 + \dfrac{\|\widetilde{\mathbf{h}}_{\pi(1)}\|^2}{P}} = \frac{\vartheta^2 P \|\widetilde{\mathbf{h}}_{\pi(1)}\|^2}{\vartheta^2 P \dfrac{\left| \widetilde{\mathbf{h}}_{\pi(1)}^H \widetilde{\mathbf{h}}_{\pi(2)} \right|^2}{\|\widetilde{\mathbf{h}}_{\pi(1)}\|^2} + 1},$$

$$\Delta_3 = \frac{\vartheta^2 P \|\widetilde{\mathbf{h}}_{\pi(2)}\|^4}{\|\widetilde{\mathbf{h}}_{\pi(2)}\|^2} = \vartheta^2 P \|\widetilde{\mathbf{h}}_{\pi(2)}\|^2.$$

Note that the preceding results are quite similar to the corresponding SINR and SNR expressions under the perfect channel estimation model considered in Section II. As different from the perfect CSI scenario, we have the estimated channel vectors and P is replaced with $\vartheta^2 P$ under the imperfect CSI case. Since $\mathbf{h}_k$ and $\widetilde{\mathbf{h}}_k$ are identically distributed for $k \in \{1, 2\}$, we can directly use Theorem 1 here by a simple substitution of $\vartheta^2 P$ for P. This justifies the above-mentioned switching strategy between the two decoding approaches under the imperfect CSI scenario.

V. NUMERICAL RESULTS

In this section, the proposed hybrid scheme is compared with the sole SDMA- and NOMA-based approaches in terms of the sum rate and the outage probability. We assume $\sigma_1^2 = 0$ dB and define SNR as P/N_0 in all the figures. Simulation parameters are tabulated in Table 1 where the abbreviation N/A stands for the phrase not applicable.

The three techniques are compared in Fig. 2 with regard to their sum rate performances. We separately consider three SNR values together with $\sigma_2^2 = -35$ dB and varying M. It is clear that the superiority order between the SDMA- and NOMA-based methods changes depending on the SNR of the users and the value of M. When SNR = 20 dB, the NOMA decoding scheme outperforms the SDMA decoding scheme. On the other hand, the SDMA decoding technique performs better than the NOMA decoding technique when SNR = 40 dB. The two techniques behave similarly for SNR = 30 dB while NOMA slightly performs better for $M \leq 4$. The sum rates of the relevant techniques are

compared in Fig. 3 for varying SNR values. For the cell-edge user, we use two different σ_2^2 values given by -30 dB and -40 dB where we adopt $M = 2$ and $M = 6$ in the former and latter cases, respectively. When $M = 2$ and $\sigma_2^2 = -30$ dB, the SDMA decoding performs better than the NOMA decoding for SNR ≥ 32.5 dB. On the other hand, the SDMA-based approach yields larger sum rate than the NOMA-based approach for SNR ≥ 35 dB when $M = 6$ and $\sigma_2^2 = -40$ dB. It is clear in both Figs. 2 and 3 that the hybrid algorithm tracks the better of the other two schemes and offers the best choice by retaining the advantages of both methods. By setting $R_k^{\text{hybrid}} = R_k^{\text{SDMA}} = R_k^{\text{NOMA}} = R_{kt}$ for $k \in \{1, 2\}$, the outage probabilities of the relevant schemes are illustrated in Fig. 4 for $M = 2$. The performance of minimum mean square error (MMSE) receive beamforming is also plotted as a benchmark. We separately examine two scenarios. We set $\{\sigma_1^2, \sigma_2^2\} = \{0, -30\}$ dB and $\{R_{1t}, R_{2t}\} = \{8, 1\}$ bits/s/Hz in the first case. Also, in the second scenario, we use $\{\sigma_1^2, \sigma_2^2\} = \{0, -40\}$ dB and $\{R_{1t}, R_{2t}\} = \{8, 0.5\}$ bits/s/Hz. For the first case, the NOMA-based scheme performs worst and exhibits a near-constant outage probability as SNR increases. In this case, the hybrid method clearly outperforms the other techniques and offers a 5 dB improvement in the SNR of both users as compared to the SDMA-based approach for an outage probability of 10^{-3}. The NOMA-based scheme performs better than the SDMA-based technique when SNR < 55 dB in the second scenario. As before, the hybrid scheme attains the lowest outage probability and, compared with its competitors, achieves a 5 dB enhancement in the users' SNR values for an outage probability of 10^{-3}. The hybrid scheme outperforms MMSE beamforming to a great extent under both scenarios. In Fig. 5, $F_{\Omega}(P)$ is plotted for $M \in \{2, 6\}$ and distinct σ_2^2 values. Note that the upper half of Fig. 5 corresponds to the region for which the probability that the SDMA-based approach performs better than the NOMA-based approach is greater than one half and vice versa. In addition, the high degree of match between the simulated and analytical results in Figs. 3, 4, and 5 corroborates the analytical derivations in Section III. Assuming possibly imperfect CSI at the BS, we compare the outage probabilities of the relevant approaches in Fig. 6 for $\sigma_2^2 = -30$ dB and $\{R_{1t}, R_{2t}\} = \{4, 0.5\}$ bits/s/Hz based on the estimation model in (26). In order to observe the effect of
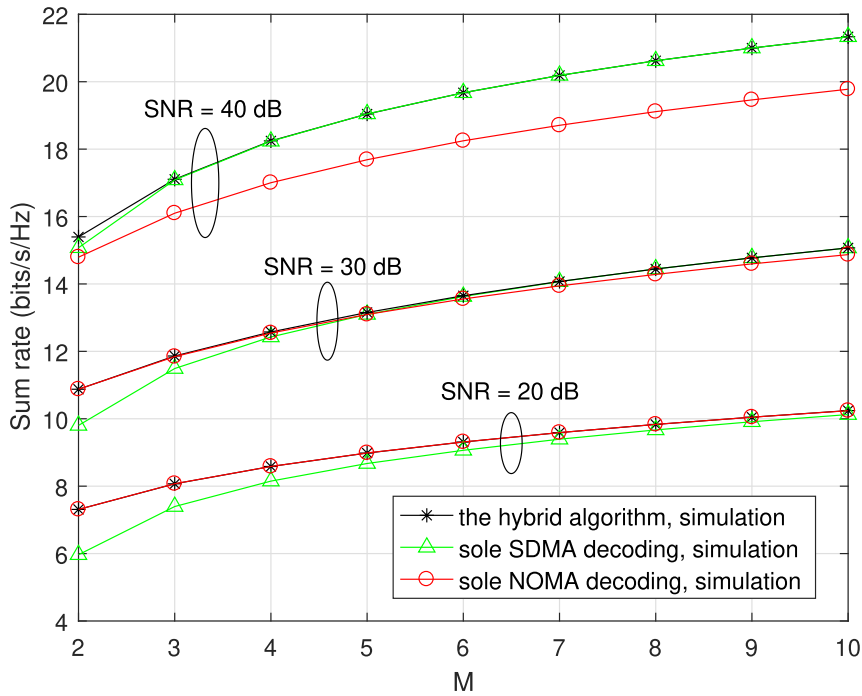
FIGURE 2. The sum rate comparison of the relevant schemes for $\sigma_1^2 = 0$ dB, $\sigma_2^2 = -35$ dB, SNR = {20, 30, 40} dB, and varying M.
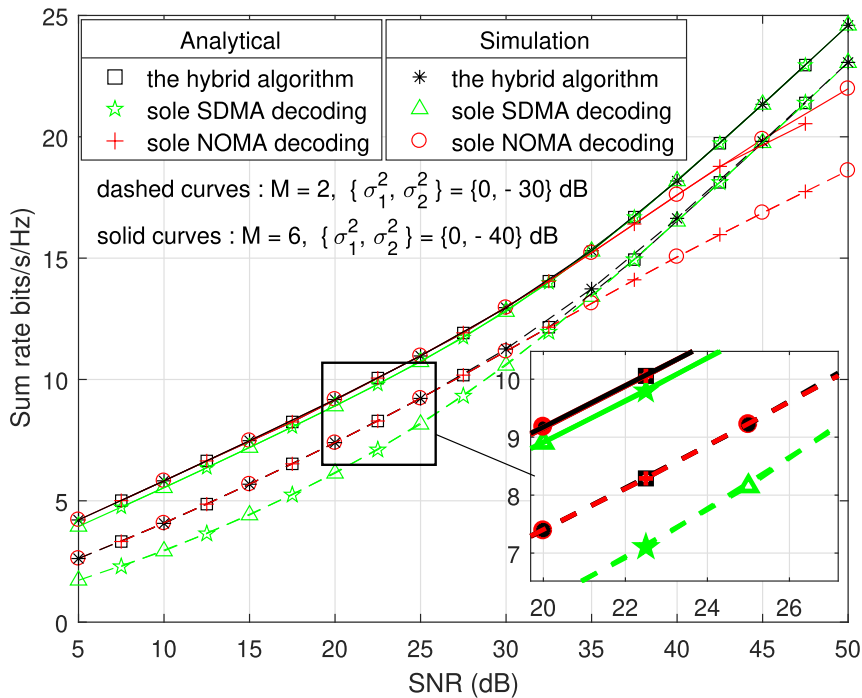

FIGURE 3. The sum rate comparison of the relevant schemes for varying SNR with $M = 2$, $\{\sigma_1^2, \sigma_2^2\} = \{0, -30\}$ dB and $M = 6$, $\{\sigma_1^2, \sigma_2^2\} = \{0, -40\}$ dB.

the imperfect channel estimation on the outage probability, we consider $\vartheta = \{0.99, 0.95\}$ as well as $\vartheta = 1$, i.e., the perfect CSI case. It turns out that the outage probability performance strictly depends on the channel estimation quality for all three schemes. Even when the estimated and true channel vectors are strongly correlated, i.e., $\vartheta = 0.99$, all three schemes seriously suffer exhibiting an error floor before reaching operational outage probability levels. In this case,
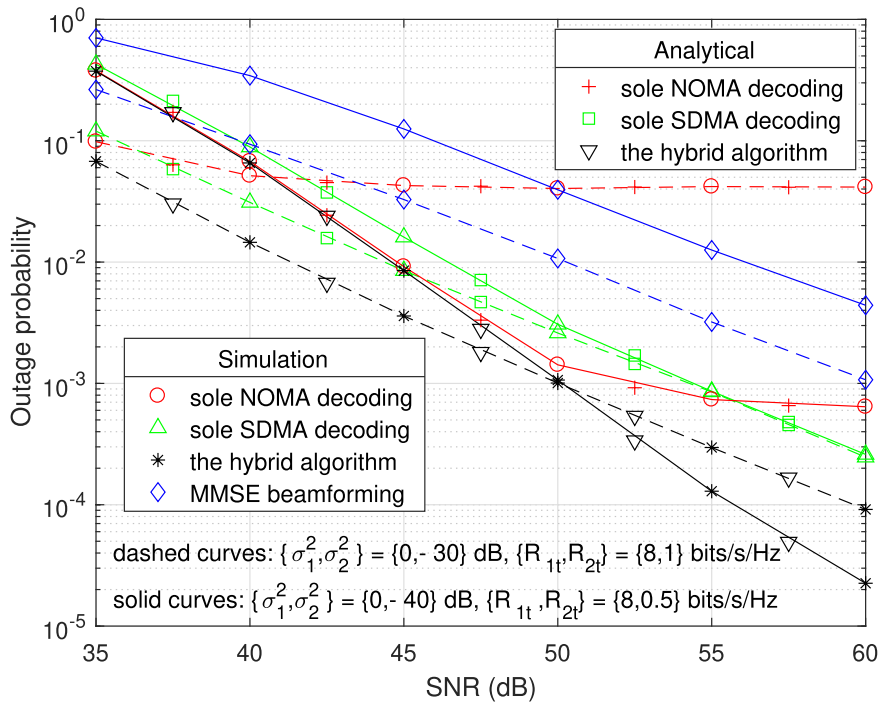
FIGURE 4. The outage probability comparison of the relevant schemes for $M = 2$ where the dashed and solid curves respectively represent the scenarios with $\{\sigma_1^2, \sigma_2^2\} = \{0, -30\}$ dB, $\{R_{1t}, R_{2t}\} = \{8, 1\}$ bits/s/Hz and $\{\sigma_1^2, \sigma_2^2\} = \{0, -40\}$ dB, $\{R_{1t}, R_{2t}\} = \{8, 0.5\}$ bits/s/Hz.
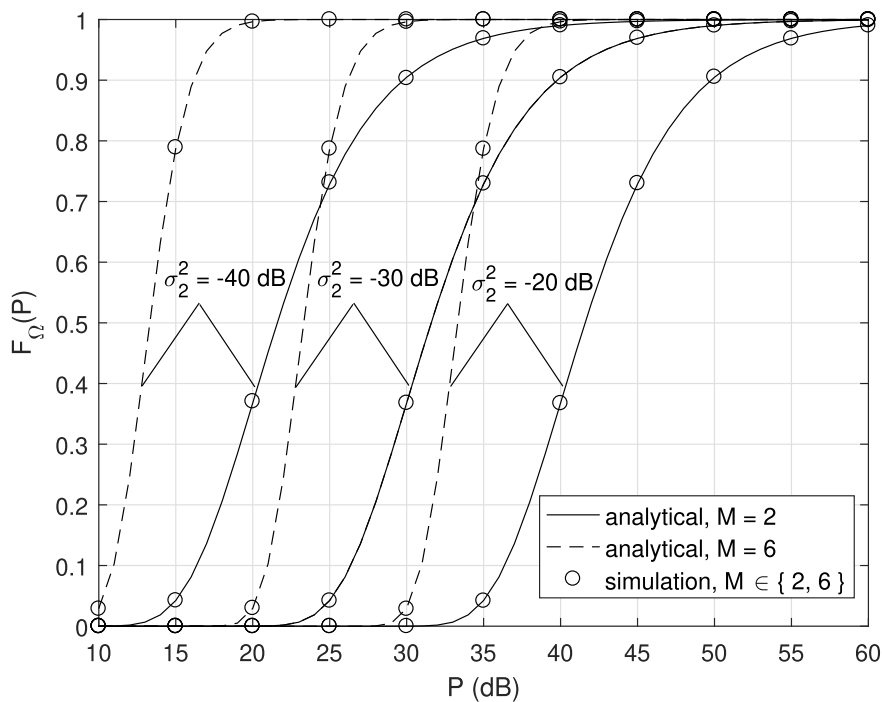

FIGURE 5. $F_{\Omega}(P)$ for $M \in \{2, 6\}$, $\sigma_1^2 = 0$ dB, and various σ_2^2 values.

the outage probability is dominantly prevailed by the channel estimation errors and increasing the transmit power may not bring about any benefit in terms of outage probability. As the channel estimation quality reduces further, all three methods tend to exhibit quite similar performances. In all cases, the proposed Hybrid algorithm achieves the best performance.
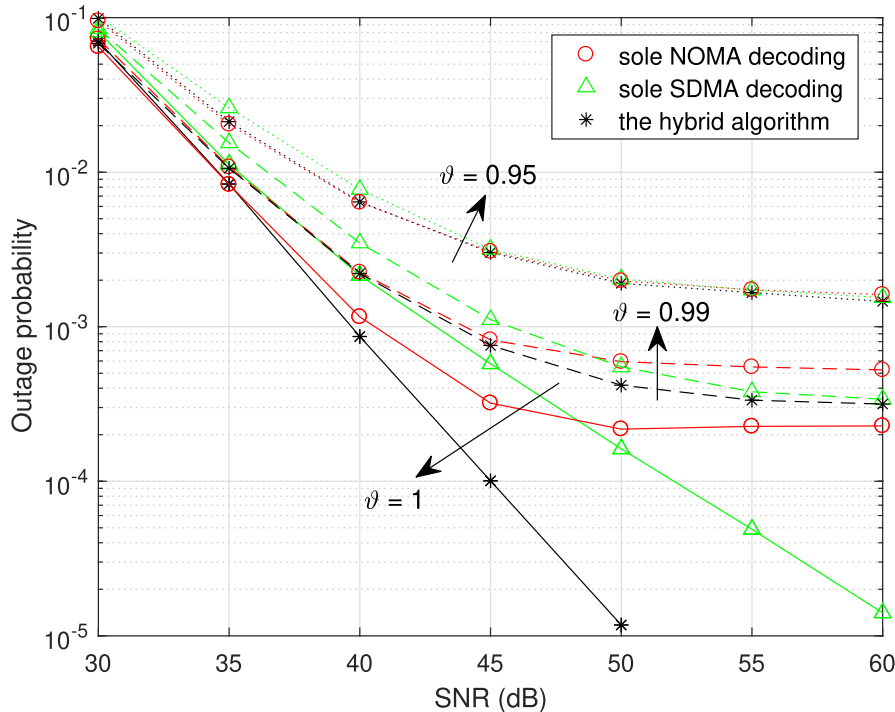
FIGURE 6. The outage probability comparison of the relevant schemes under channel estimation errors for $M = 2$, $\sigma_1^2 = 0$ dB, $\sigma_2^2 = -30$ dB, and $\{R_{1t}, R_{2t}\} = \{4, 0.5\}$ bits/s/Hz.

VI. CONCLUSION

An uplink cellular communications scenario has been investigated by assuming that two single-antenna users without any CSI are desired to communicate simultaneously with a multi-antenna BS on the same frequency band. We have presented a hybrid orthogonal/non-orthogonal multiple access scheme by properly combining NOMA and SDMA techniques where power domain and spatial degrees of freedom are respectively utilized in the latter and former scenarios for multiplexing the users' symbols. It is illustrated that such a combination can yield significant gains (as large as 5 dB) in terms of the users' SNR (or SINR) values with respect to average sum rate and outage probability criteria under both perfect and imperfect CSI cases. Further, the relevant methods are statistically analyzed by deriving novel CDF expressions to be used for the evaluations of average sum rate and outage probability. The obtained analytical results for the conventional NOMA and SDMA approaches are also novel and add to the original contribution of this study. The current study lays the foundations and the introduced hybrid technique can be extended for other scenarios with more than two users under distinct channel fading characteristics.

REFERENCES

[1] *IMT Traffic Estimates for the Years 2020 to 2030*, document ITU-R M.2370-0, 2015.

[2] H. Viswanathan and P. E. Mogensen, "Communications in the 6G era," *IEEE Access*, vol. 8, pp. 57063–57074, 2020.

[3] Y. Saito, Y. Kishiyama, A. Benjebbour, T. Nakamura, A. Li, and K. Higuchi, "Non-orthogonal multiple access (NOMA) for cellular future radio access," in *Proc. IEEE 77th Veh. Technol. Conf.*, Dresden, Germany, Jun. 2013, pp. 1–5.

[4] Y. Liu, S. Zhang, X. Mu, Z. Ding, R. Schober, N. Al-Dhahir, E. Hossain, and X. Shen, "Evolution of NOMA toward next generation multiple access (NGMA) for 6G," *IEEE J. Sel. Areas Commun.*, vol. 40, no. 4, pp. 1037–1071, Apr. 2022.

[5] *Study on Downlink Multiuser Superposition Transmission*, 3GPP, document TD RP-150496, Mar. 2015.

[6] *Study on Non-Orthogonal Multiple Access (NOMA) for NR*, 3GPP, document TR 38.812, Dec. 2018.

[7] S. M. R. Islam, M. Zeng, and O. A. Dobre, "NOMA in 5G systems: Exciting possibilities for enhancing spectral efficiency," 2017, *arXiv:1706.08215*.

[8] G. Lee, Y. Sung, and M. Kountouris, "On the performance of random beamforming in sparse millimeter wave channels," *IEEE J. Sel. Topics Signal Process.*, vol. 10, no. 3, pp. 560–575, Apr. 2016.

[9] Z. Ding, P. Fan, and H. V. Poor, "Random beamforming in millimeter-wave NOMA networks," *IEEE Access*, vol. 5, pp. 7667–7681, 2017.

[10] J. Mietzner, R. Schober, L. Lampe, W. Gerstacker, and P. Hoeher, "Multiple-antenna techniques for wireless communications—A comprehensive literature survey," *IEEE Commun. Surveys Tuts.*, vol. 11, no. 2, pp. 87–105, 2nd Quart., 2009.

[11] S. Yang and L. Hanzo, "Fifty years of MIMO detection: The road to large-scale MIMOs," *IEEE Commun. Surveys Tuts.*, vol. 17, no. 4, pp. 1941–1988, 4th Quart., 2015.

[12] A. Ghosh, A. Maeder, M. Baker, and D. Chandramouli, "5G evolution: A view on 5G cellular technology beyond 3GPP release 15," *IEEE Access*, vol. 7, pp. 127639–127651, 2019.

[13] B. Clerckx, Y. Mao, R. Schober, E. A. Jorswieck, D. J. Love, J. Yuan, L. Hanzo, G. Y. Li, E. G. Larsson, and G. Caire, "Is NOMA efficient in multi-antenna networks? A critical look at next generation multiple access techniques," *IEEE Open J. Commun. Soc.*, vol. 2, pp. 1310–1343, 2021.

[14] Q. Yang, H.-M. Wang, D. W. K. Ng, and M. H. Lee, "NOMA in downlink SDMA with limited feedback: Performance analysis and optimization," *IEEE J. Sel. Areas Commun.*, vol. 35, no. 10, pp. 2281–2294, Oct. 2017.

[15] Z. Ding, "NOMA beamforming in SDMA networks: Riding on existing beams or forming new ones?" *IEEE Commun. Lett.*, vol. 26, no. 4, pp. 868–871, Apr. 2022.

[16] Z. Ding, R. Schober, and H. V. Poor, "NOMA-based coexistence of near-field and far-field massive MIMO communications," *IEEE Wireless Commun. Lett.*, vol. 12, no. 8, pp. 1429–1433, Aug. 2023.

[17] L. Zhu, Z. Xiao, X.-G. Xia, and D. Oliver Wu, "Millimeter-wave communications with non-orthogonal multiple access for B5G/6G," *IEEE Access*, vol. 7, pp. 116123–116132, 2019.

[18] I. Khaled, C. Langlais, A. El Falou, M. Jezequel, and B. ElHasssan, "Joint SDMA and power-domain NOMA system for multi-user mm-wave communications," in *Proc. Int. Wireless Commun. Mobile Comput. (IWCMC)*, Jun. 2020, pp. 1112–1117.

[19] B. Clerckx, Y. Mao, R. Schober, and H. V. Poor, "Rate-splitting unifying SDMA, OMA, NOMA, and multicasting in MISO broadcast channel: A simple two-user rate analysis," *IEEE Wireless Commun. Lett.*, vol. 9, no. 3, pp. 349–353, Mar. 2020.

[20] S. Naser, P. C. Sofotasios, L. Bariah, W. Jaafar, S. Muhaidat, M. Al-Qutayri, and O. A. Dobre, "Rate-splitting multiple access: Unifying NOMA and SDMA in MISO VLC channels," *IEEE Open J. Veh. Technol.*, vol. 1, pp. 393–413, 2020.

[21] Z. Ding and H. V. Poor, "A simple design of IRS-NOMA transmission," *IEEE Commun. Lett.*, vol. 24, no. 5, pp. 1119–1123, May 2020.

[22] S. Yang, J. Zhang, W. Xia, Y. Ren, H. Yin, and H. Zhu, "A unified framework for distributed RIS-aided downlink systems between MIMO-NOMA and MIMO-SDMA," *IEEE Trans. Commun.*, vol. 70, no. 9, pp. 6310–6324, Sep. 2022.

[23] H. Al-Obiedollah, A. Hayajneh, H. B. Salameh, K. Cumanan, and A. M. Y. Al-Nimrat, "On the performance of multi-carrier SDMA-NOMA CR-based systems," in *Proc. 8th Int. Conf. Softw. Defined Syst. (SDS)*, Gandia, Spain, Dec. 2021, pp. 1–5.

[24] J. Maeng, M. K. Dahouda, and I. Joe, "Optimal power allocation with sectored cells for sum-throughput maximization in wireless-powered communication networks based on hybrid SDMA/NOMA," *Electronics*, vol. 11, no. 6, p. 844, Mar. 2022.

[25] H. Kong, M. Tan, M. Lin, M. Cheng, W.-P. Zhu, and T. de Cola, "Hybrid multiple access transmission in satellite-aerial-terrestrial networks," *IEEE Commun. Lett.*, vol. 26, no. 9, pp. 2146–2150, Sep. 2022.

[26] H. Kong, M. Lin, L. Han, W.-P. Zhu, Z. Ding, and M.-S. Alouini, "Uplink multiple access with semi-grant-free transmission in integrated satellite-aerial-terrestrial networks," *IEEE J. Sel. Areas Commun.*, vol. 41, no. 6, pp. 1723–1736, June 2023.

[27] Z. Gao, X. Zhou, J. Zhao, J. Li, C. Zhu, C. Hu, P. Xiao, S. Chatzinotas, D. W. K. Ng, and B. Ottersten, "Grant-free NOMA-OTFS paradigm: Enabling efficient ubiquitous access for LEO satellite Internet-of-Things," *IEEE Netw.*, vol. 37, no. 1, pp. 18–26, Jan. 2023.

[28] B. He, H. Wang, H. Wang, R. Song, and Q. Tai, "Novel structure for uplink mmWave massive MIMO-HBF-NOMA systems," in *Proc. IEEE Wireless Commun. Netw. Conf. (WCNC)*, Mar. 2023, pp. 1–5.

[29] Z. Yang, Z. Ding, P. Fan, and G. K. Karagiannidis, "On the performance of non-orthogonal multiple access systems with partial channel information," *IEEE Trans. Commun.*, vol. 64, no. 2, pp. 654–667, Feb. 2016.

[30] M. A. Sedaghat and R. R. Müller, "On user pairing in uplink NOMA," *IEEE Trans. Wireless Commun.*, vol. 17, no. 5, pp. 3474–3486, May 2018.

[31] S. Loyka and F. Gagnon, "Performance analysis of the V-BLAST algorithm: An analytical approach," *IEEE Trans. Wireless Commun.*, vol. 3, no. 4, pp. 1326–1337, Jul. 2004.

[32] K. Scharnhorst, "Angles in complex vector spaces," *Acta Applicandae Math.*, vol. 69, no. 1, pp. 95–103, Oct. 2001.

[33] A. Goldsmith, "On the optimality of multiantenna broadcast scheduling using zero-forcing beamforming," *IEEE J. Sel. Areas Commun.*, vol. 24, no. 3, pp. 528–541, Mar. 2006.

[34] T. Yoo, N. Jindal, and A. Goldsmith, "Multi-antenna downlink channels with limited feedback and user selection," *IEEE J. Sel. Areas Commun.*, vol. 25, no. 7, pp. 1478–1491, Sep. 2007.

[35] W. Ni, Z. Chen, H. Suzuki, and I. B. Collings, "On the performance of semi-orthogonal user selection with limited feedback," *IEEE Commun. Lett.*, vol. 15, no. 12, pp. 1359–1361, Dec. 2011.

[36] M. Abramowitz and I. A. Stegun, *Handbook of Mathematical Functions with Formulas, Graphs, and Mathematical Tables*, 10th ed. New York, NY, USA: Dover, 1972.

[37] H. A. David and H. N. Nagaraja, *Order Statistics*, 3rd ed. Hoboken, NJ, USA: Wiley, 2003.

SERDAR ÖZYURT received the B.Sc. degree in electrical and electronics engineering from Sakarya University, Turkey, in 2001, the M.Sc. degree in electronics engineering from the Gebze Institute of Technology, Turkey, in 2005, and the Ph.D. degree in electrical engineering from The University of Texas at Dallas, USA, in 2012. He is currently an Associate Professor with the Department of Electrical and Electronics Engineering, Ankara Yıldırım Beyazıt University, Ankara, Turkey. His current research interests include multi-antenna multiuser communications, diversity techniques, spatial multiplexing methods, and multi-carrier communications.

ERIC PIERRE SIMON received the M.S. degree in electronics engineering from the Superior School of Electronics, Lyon, France, in 1999, and the Ph.D. degree in signal processing and communications from the National Polytechnic Institute of Grenoble (INPG), Grenoble, France, in 2004. In 2005, he was a Teaching Assistant with INPG. In 2006, he joined one of the France Telecom Research and Development Laboratories as a Postdoctoral Fellow. He is currently an Associate Professor at the IEMN Laboratory (CNRS, UMR 8520), University of Lille, France. His current research interests include multi-antenna communications, multiple access techniques such as NOMA, and machine learning for communications.

MURAT TORLAK (Senior Member, IEEE) received the M.S. and Ph.D. degrees in electrical engineering from The University of Texas at Austin, in 1995 and 1999, respectively. Since August 1999, he has been with the Department of Electrical and Computer Engineering, The University of Texas at Dallas, where he has been promoted to the rank of a Full Professor. He served as a rotating Program Director at the U.S. National Science Foundation (NSF) between 2020 to 2023. His current research interests include experimental verification of wireless networking systems, cognitive radios, millimeter-wave automotive radars, millimeter-wave imaging systems, and interference mitigation in radio telescopes. He was the General Chair of the Symposium on Millimeter-Wave Imaging and Communications, IEEE GlobalSIP Conference, in 2013. He was an Associate Editor of the IEEE TRANSACTIONS ON WIRELESS COMMUNICATIONS, from 2008 to 2013. He was the Guest Co-Editor for the Special Issues on Recent Advances in Automotive Radar Signal Processing of IEEE JOURNAL OF SELECTED TOPICS IN SIGNAL PROCESSING (JSTSP), in 2021.

• • •